Pergamon

Int. J. Solids Structures Vol. 34, No. 15, pp. 1849–1871, 1997

0020–7683/97 $17.00 + .00

PII: S0020–7683(96)00130–8

NEAR-TIP MODE-I ELASTIC FIELDS IN BIMATERIAL LAYERED SYSTEMS

M. JHA, P. G. CHARALAMBIDES
Department of Mechanical Engineering, The University of Maryland, Baltimore County, Baltimore, MD 21228-5398, U.S.A.

and

R. BALLARINI
Department of Civil Engineering, Case Western Reserve University, Cleveland, OH 44106, U.S.A.

(*Received* 15 *February* 1996)

Abstract—The micromorphic stress fields in the near-tip region of a Mode-I semi-infinite crack embedded in an infinite elastic bimaterial layered system are investigated. The local and global features of the micromorphic stresses in the heterogeneous near-tip domain are captured through an approximate analytical model *vis-à-vis* a two-dimensional plane strain finite element model. The studies are carried out within a heterogeneous *cut-out* region surrounding the physical crack-tip wherein alternating *matrix* and *fiber* layers are positioned perpendicular to the crack plane. The approximate analytical model is developed by postulating a general form of displacement field that is obtained by the superposition of the applied homogenized near-tip field and a family of kinematically admissible unit-cell micro-displacements. While preserving the aggregate response of the material, these micro-displacements take into account the effects of material micro-structure. The results indicate that the microstress field in the immediate vicinity of the crack-tip exhibits an $r^{-1/2}$ singularity when the crack-tip is located entirely within the matrix phase and lies sufficiently away from the adjacent interfaces. The structure of the stress field in the matrix region surrounding the crack-tip corresponds to the universal isotropic field dominated by the tip stress intensity factor. In the far-field region (radial distance greater than one unit-cell thickness), the continuous stress components σ_{xx} and σ_{xy} are found to be dominated by the orthotropic stress intensity factor and found to be in good agreement with their homogeneous orthotropic counterparts. As expected, the discontinuous stress component σ_{yy} is found to exhibit strong dependency on the material heterogeneity. While σ_{yy} is dominated by the applied orthotropic stress intensity factor, it is described by a discontinuous spatial eigen-function which has been obtained with the aid of the analytical approximate model. Several parameter studies are presented and implications on the mode-I brittle fracture in layered systems are discussed. © 1997 Elsevier Science Ltd.

1. INTRODUCTION

In recent years, layered composites have received increasing attention due to their potentially superior directional stiffness, strength and toughness properties. Ceramic and metal matrix layered systems are primarily considered for high temperature applications whereas unidirectionally fiber reinforced laminates are often used by the aerospace, automotive and durable goods industries mainly due to their superior mechanical properties. In addition to the above applications, layered morphologies are also used in component joining and protective coating systems, electronic structures such as multi-layer capacitors and micro-chip applications, and in advanced fiber optics for telecommunications and information technology. While exhibiting desirable mechanical characteristics, layered monolithic and fiber reinforced composite laminates may also exhibit rather complex life-limiting failures. Several types of failures associated with multilayered systems have been observed and reported in the literature. The prominent modes of failure in layered systems include mixed-mode delamination, transverse cracking of low strength layers, thin film decohesion, spalling and blistering of thin films, crack tunneling and film or substrate cracking. In periodically layered materials, a planar crack, under cyclic and/or environmental loadings, may propagate sub-critically through several layers forming a macroscopically well defined crack under mode-I loading. In brittle/ductile layered systems, mode-I cracks may propagate

perpendicular to the layers in the brittle phase while bridged by the ductile layers. The crack propagation in these systems is often achieved through renucleation of cracks in the brittle layers ahead of the crack-tip while the metal layers in the crack wake undergo plastic yielding and potentially experience debonding and separation from the adjacent brittle matrix [Dalgleish *et al.* (1989), Cao and Evans (1991), Deve and Maloney (1991)].

For a crack approaching a bimaterial interface at a 90-degree angle, Suresh *et al.* (1992) showed experimentally and Sugimura *et al.* (1995) showed analytically that for brittle systems, the near-tip *crack driving force* or the elastic energy release rate, depends strongly on the stiffness of the layer ahead of the crack tip relative to the stiffness of the layer containing the crack-tip. Several studies [He and Hutchinson (1989), Martinez and Gupta (1993), Tullock *et al.* (1994)] have shown that the competition between crack deflection and penetration at the interface and subsequent evolution of fracture strongly depends on the properties of the constituent layers, the properties of the interface and the mechanics dominating the near-tip region.

The problem of a planar crack terminating perpendicular to the interface between two isotropic half planes was studied by Zak and Williams (1963), Swenson and Rau (1970), Erdogan and Biricikoglu (1973), and Cook and Erdogan (1972). The near-tip mechanics of a crack terminating at the interface between two elastic anisotropic half planes were studied by Gupta *et al.* (1992), Ting and Hoang (1984) and Erdogan (1972). Finite geometry effects for isotropic bimaterials containing cracks of various configurations were addressed by Lu and Erdogan (1983) and by Ballarini and Luo (1991). A comprehensive survey of solutions for mixed-mode cracking in layered systems has been reported by Hutchinson and Suo (1992). Zak and Williams (1963) showed that for cracks terminating at bimaterial interfaces the power of the singularity dominating the near-tip stress fields has the form $r^{-\gamma}$ with $\gamma \neq \frac{1}{2}$ and $0 < \gamma < 1$ which hinders the direct use of a critical energy release rate criterion in assessing initiation of crack growth. However, Delale and Erdogan (1988) and Erdogan *et al.* (1991) showed that the deviation from the $r^{-1/2}$ singularity can be overcome by introducing gradient material properties within a small interface region. Compared to the large volume of research in characterizing the near-tip fields and fracture of two layer systems, relatively limited research has been reported for the analytically intractable problem of periodically layered systems containing cracks perpendicular to the layers. Recently, Ballarini *et al.* (1995) and Fish *et al.* (1993) presented results from numerical studies on the near-tip mechanics of mode-I cracking in periodically layered bimaterial systems.

Motivated by the immense practical applications of layered systems, this work is devoted to the development of an approximate analytical model aimed at capturing with sufficient accuracy the local and global features of the near-tip fields for cracks embedded at 90-degree to the interfaces in periodically layered systems. The model predictions are compared with refined finite element solutions obtained by solving the related boundary value problem involving a heterogeneous near-tip region *cut-out* from the periodically layered system. The formulation of the problem is presented in Section 2. The development of the analytical model is fully described in Section 3 and the related finite element model is presented in Section 4. The results from the analytical model and finite element analyses are reported in Section 5 and discussed in Section 6 which also includes parametric studies and implications on brittle fracture of the layered systems under consideration. The paper concludes in Section 7 with a summary of the salient findings of this work.

2. STATEMENT OF THE PROBLEM

The problem addressed in this work is shown in Fig. 1, where a semi-infinite crack embedded in an otherwise infinite perfectly bonded bimaterial layered system is shown. The bimaterial layered system is comprised of alternating *matrix* and *fiber* layers positioned perpendicular to the crack plane. This layered morphology may be used to represent either a fiber reinforced [0/90] cross-ply laminate or a bimaterial periodically layered system. In this study, the materials for the two phases were taken to be homogeneous and linearly elastic. The thicknesses of the matrix and the fiber phases are taken to be l_m and l_f,

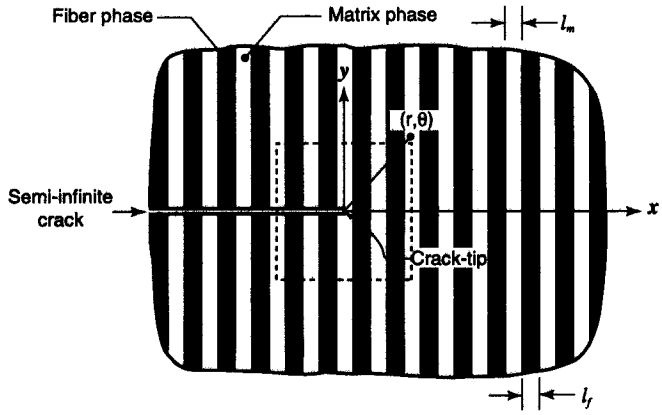

Fig. 1. A semi-infinite crack in an infinite periodically layered bimaterial system.

respectively, while $l = l_m + l_f$ represents the thickness of a fiber/matrix unit-cell. The cartesian coordinate system is chosen with its origin located at the crack-tip as shown in Fig. 1. The loading is assumed such that overall mode-I conditions prevail. The crack surfaces are traction free and the crack-tip is assumed to be ideally sharp. Plane strain conditions are considered. For the approximate analytical model, the crack-tip is assumed to be in the matrix phase at mid-distance between the adjacent fiber layers. In formulating the near-tip finite element model, a *cut-out* region surrounding the physical crack-tip as indicated by the dashed lines will be considered.

3. ANALYTICAL MODEL

The model is based on the non-standard analysis approach of Wozniak (1987) for problems with periodic material structure, wherein the displacements are postulated in terms of the homogenized orthotropic displacements augmented by a family of kinematically admissible unit-cell local displacements. Here it is emphasized that the effects of the geometrically non-periodic macrocrack enter into the solution through the homogenized asymptotic fields. As such, the fundamental assumptions used by Wozniak (1987) in formulating the non-standard analysis for micro-periodic material structure are valid. In this approach, the local displacements are cast in terms of a unit-cell shape function which is known *a priori* and some unknown micromorphic parameter functions which depend on the degree of material heterogeneity and the lamination morphology via the layer volume fractions. While the micromorphic parameters describe quantitatively the effects of the micro-periodic material structure, the shape function describes the expected qualitative character of these effects. The unknown micromorphic parameters are obtained by invoking an energy minimization technique. The homogeneous domain solution is then obtained by solving the Navier displacement field equations subjected to homogenized boundary conditions.

3.1. *Deformation hypothesis*

Assuming that the global mechanical response of the layered system conforms to that of the homogenized orthotropic linear elastic model, the displacement field can be postulated in terms of the applied homogenized near-tip displacement field augmented by kinematically admissible unit-cell local displacements [see, for example, Wozniak (1987), Matysiak and Wozniak (1987) and Kaczynski and Matysiak (1989)]. As such, under plane strain conditions, the actual displacement vector $\mathbf{u} = \{u, v\}^{\mathrm{T}}$ can be approximated as the sum of the macro-displacements $\bar{\mathbf{u}} = \{\bar{u}, \bar{v}\}^{\mathrm{T}}$ and the local displacements $\mathbf{u}^l = \{u^l, v^l\}^{\mathrm{T}}$ as follows:

$$u(x, y) = \bar{u}(x, y) + u^l(x, y),$$
$$v(x, y) = \bar{v}(x, y) + v^l(x, y). \tag{1}$$

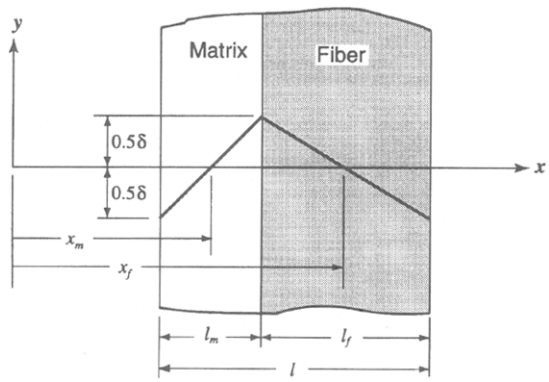

Fig. 2. A linear shape function profile within a matrix/fiber unit-cell.

While $\bar{\mathbf{u}}$ preserves the aggregate orthotropic response, $\mathbf{u}^l = \{u^l, v^l\}^T$ takes into account the effects of micro-periodic material structure. The micro-displacements can be expressed in terms of a unit-cell shape function $h(x)$ and the micromorphic parameter functions $g_i(x, y)$ $(i = 1, 2)$ as follows:

$$u^l(x, y) = g_1(x, y)h(x),$$
$$v^l(x, y) = g_2(x, y)h(x). \tag{2}$$

The shape function $h(x)$ is an *a priori* known l-periodic function which satisfies the following periodicity and local equilibrium conditions:

$$h(x) = h(x+l),$$
$$\int_x^{x+1} h(x)\,dx = 0. \tag{3}$$

The unknown functions $g_i(x, y)$ are called the micromorphic parameters and they are assumed to be smooth functions of x and y.

Any function satisfying eqn (3) can be taken as a candidate for the shape function and a homogenized model associated with the selected shape function can be obtained. This situation is analogous to that of the finite element method, where also we deal with different choices of the shape functions. The choice of a particular shape function may then be made based on the simplicity and accuracy of the homogenized model. In this study, several shape functions were tested and it was found that the linear shape function gave the most consistent and accurate results. A sectionally linear shape function for the bilayer periodic laminated composite is shown in Fig. 2. This shape function can be expressed as:

$$h(x) = \begin{cases} \dfrac{1}{v_m}(x - x_m)\dfrac{\delta}{l} & \text{for } (x_m - 0.5l_m) \leqslant x \leqslant (x_m + 0.5l_m) \\ -\dfrac{1}{v_f}(x - x_f)\dfrac{\delta}{l} & \text{for } (x_f - 0.5l_f) \leqslant x \leqslant (x_f + 0.5l_f) \end{cases} \tag{4}$$

where $v_m = l_m/l$, $v_f = l_f/l$ and $l = l_m + l_f$. Obviously, v_m and v_f represent the volume fractions of the matrix and the fiber layers respectively. As will be shown later in this work, the governing equations and ensuing homogenized material constants are independent of the amplitude δ of the shape function. As such, the value of δ is chosen to be the matrix layer thickness in the present study.

For the postulated plane deformation field (1), the linearized strain–displacement relations take the following form:

$$\varepsilon_{xx} = \bar{\varepsilon}_{xx} + hg_{1,x} + g_1 h_{,x}$$
$$\varepsilon_{yy} = \bar{\varepsilon}_{yy} + hg_{2,y}$$
$$\gamma_{xy} = \bar{\gamma}_{xy} + h(g_{1,y} + g_{2,x}) + g_2 h_{,x}. \tag{5}$$

It is worth mentioning here that in the above equations the shape function $h(x)$ and its derivative are evaluated locally within the appropriate unit-cell consistent with the coordinate x (see Fig. 2).

3.2. *Governing equations*

The generalized stress–strain relations for a linear elastic material are given by

$$\sigma_i = c_{ij}\varepsilon_j \tag{6}$$

where $i, j = 1, 2, \ldots, 6$ and summation from 1 to 6 is implied over the repeated index j. The above equations are derived using contracted notation such that $\{\varepsilon_i\} = [\varepsilon_{xx}, \varepsilon_{yy}, \varepsilon_{zz}, \gamma_{yz}, \gamma_{zx}, \gamma_{xy}]^T$, $\{\sigma_i\} = [\sigma_{xx}, \sigma_{yy}, \sigma_{zz}, \sigma_{zy}, \sigma_{zx}, \sigma_{xy}]^T$ and $[c_{ij}]$ is the six-by-six symmetric elastic stiffness matrix.

The strain energy density ϕ for a linear elastic body under plane conditions is given by:

$$\phi = \tfrac{1}{2}\sigma_i\varepsilon_i = \tfrac{1}{2}c_{ij}\varepsilon_i\varepsilon_j \quad i,j = 1,2,6 \tag{7}$$

where summation is implied over the repeated indices. The average energy density in the unit-cell of a layered system can be defined as:

$$\bar{\phi} = \frac{1}{l}\int_x^{x+l} \phi \, \mathrm{d}x. \tag{8}$$

For an integrable real valued l-periodic function φ, i.e., $\varphi(x) = \varphi(x+l)$, $x \in R$ we define the following auxiliary average values:

$$\langle\varphi\rangle = \frac{1}{l}\int_x^{x+l} \varphi \, \mathrm{d}x$$
$$\langle\varphi\rangle_1 = \frac{1}{l}\int_x^{x+l} \varphi h'(x) \, \mathrm{d}x$$
$$\langle\varphi\rangle_{11} = \frac{1}{l}\int_x^{x+l} \varphi h'(x)h'(x) \, \mathrm{d}x \tag{9}$$

where $h'(x) = \partial h/\partial x$. With the aid of eqns (5) and (7), the average energy density for a layered system can be obtained in terms of the macro-strains $\bar{\varepsilon}_i$, the micromorphic functions $g_i(x, y)$ and the averaged elastic properties of the stratified medium. More specifically, for a layered system comprised of either homogeneous orthotropic or isotropic layers ($c_{16} = c_{26} = 0$), the linearized average energy density is given by:

$$\bar{\phi} = \tfrac{1}{2}[\langle c_{11}\rangle\bar{\varepsilon}_1\bar{\varepsilon}_1 + 2\langle c_{12}\rangle\bar{\varepsilon}_1\bar{\varepsilon}_2 + \langle c_{22}\rangle\bar{\varepsilon}_2\bar{\varepsilon}_2 + \langle c_{66}\rangle\bar{\varepsilon}_6\bar{\varepsilon}_6]$$
$$+ [\langle c_{11}\rangle_1\bar{\varepsilon}_1 g_1 + \langle c_{12}\rangle_1\bar{\varepsilon}_2 g_1 + \langle c_{66}\rangle_1\bar{\varepsilon}_6 g_2] + \tfrac{1}{2}[\langle c_{11}\rangle_{11} g_1 g_1 + \langle c_{66}\rangle_{11} g_2 g_2] \tag{10}$$

where the averaging notation introduced in eqn (9) is used to denote various averaged elastic constants. For the bilayer unit-cell shown in Fig. 2, the auxiliary averaged elastic constants are given by:

$$\langle c_{ij}\rangle = v_m c_{ij}^m - v_f c_{ij}^f$$
$$\langle c_{ij}\rangle_1 = (\delta/l)(c_{ij}^m + c_{ij}^f)$$
$$\langle c_{ij}\rangle_{11} = (\delta/l)^2\left(\frac{c_{ij}^m}{v_m} + \frac{c_{ij}^f}{v_f}\right) \tag{11}$$

where the superscripts m and f stand for the matrix and the fiber layers, respectively. Assuming that the equivalent homogenized orthotropic medium is hyperelastic, eqn (10) can be used to obtain the stress–strain relations for the effective medium as follows:

$$\bar{\sigma}_{ij} = \frac{\partial \bar{\phi}}{\partial \bar{\varepsilon}_{ij}} \tag{12}$$

where $\bar{\sigma}_{ij}$ and $\bar{\varepsilon}_{ij}$ are the homogeneous orthotropic macro-stress and macro-strain components.

The governing equations for the macro-displacements $\bar{u}$ and $\bar{v}$ as well as the micromorphic functions $g_i(x, y)$ can be obtained through local stress equilibrium and a strain energy density minimization process for the homogenized medium. Specifically, the homogenized continuum must be in local equilibrium such that $\bar{\sigma}_{ij,j} = 0$ in the absence of body forces. Moreover, the strain energy density $\bar{\phi}$ of the homogenized continuum should attain a minimum with respect to the micromorphic functions g_1 and g_2 such that $\partial\bar{\phi}/\partial g_i = 0$ for all x, $y \in R$. Thus, for plane strain conditions and in the absence of body forces, local equilibrium and strain energy minimization yield the following governing equations:

$$\begin{aligned}
\langle c_{11}\rangle \bar{u}_{,xx} + (\langle c_{12}\rangle + \langle c_{66}\rangle)\bar{v}_{,xy} + \langle c_{66}\rangle \bar{u}_{,yy} + \langle c_{11}\rangle_1 g_{1,x} + \langle c_{66}\rangle_1 g_{2,y} &= 0\\
\langle c_{66}\rangle \bar{v}_{,xx} + (\langle c_{12}\rangle + \langle c_{66}\rangle)\bar{u}_{,xy} + \langle c_{22}\rangle \bar{v}_{,xx} + \langle c_{12}\rangle_1 g_{1,y} + \langle c_{66}\rangle_1 g_{2,x} &= 0\\
\langle c_{11}\rangle_1 \bar{u}_{,x} + \langle c_{12}\rangle_1 \bar{v}_{,y} + \langle c_{11}\rangle_{11} g_1 &= 0\\
\langle c_{66}\rangle_1 \bar{v}_{,x} + \langle c_{66}\rangle_1 \bar{u}_{,y} + \langle c_{66}\rangle_{11} g_2 &= 0.
\end{aligned} \tag{13}$$

The non-standard formulation of the elasticity problem for heterogeneous periodic layered systems is formally completed via eqns (1)–(13). The boundary conditions associated with the above governing equations can be imposed either in terms of displacements or traction. By further eliminating the micromorphic parameters $g_i(x, y)$ from eqns (13), we obtain the governing equations for the homogenized domain in terms of macro displacements and homogenized elastic constants, C_{ij}, as follows:

$$\begin{aligned}
C_{11}\bar{u}_{,xx} + (C_{12} + C_{66})\bar{v}_{,xy} + C_{66}\bar{u}_{,yy} &= 0\\
C_{66}\bar{v}_{,xx} + (C_{12} + C_{66})\bar{u}_{,xy} + C_{22}\bar{v}_{,yy} &= 0
\end{aligned} \tag{14}$$

where

$$\begin{aligned}
C_{11} &= \langle c_{11}\rangle - \frac{\langle c_{11}\rangle_1 \langle c_{11}\rangle_1}{\langle c_{11}\rangle_{11}}\\
C_{22} &= \langle c_{22}\rangle - \frac{\langle c_{12}\rangle_1 \langle c_{12}\rangle_1}{\langle c_{11}\rangle_{11}}\\
C_{12} &= \langle c_{12}\rangle - \frac{\langle c_{11}\rangle_1 \langle c_{12}\rangle_1}{\langle c_{11}\rangle_{11}}\\
C_{66} &= \langle c_{66}\rangle - \frac{\langle c_{66}\rangle_1 \langle c_{66}\rangle_1}{\langle c_{66}\rangle_{11}}.
\end{aligned} \tag{15}$$

The above quantities C_{ij} $(i, j = 1, 2 \text{ and } 6)$ with $C_{16} = C_{26} = 0$ are essentially the components

of the symmetric stiffness matrix for the homogenized continuum for which the constitutive relations of the form $\bar{\sigma}_i = C_{ij}\bar{\varepsilon}_j$ $(i,j = 1,2,6)$ apply. It is to be noted here that although $\langle c_{ij}\rangle_1$ and $\langle c_{ij}\rangle_{11}$ are dependent on (δ/l) as given by eqn (11), C_{ij} are independent of (δ/l).

3.3. *The micro mechanical fields*

For a given set of boundary conditions, the governing eqns (14) can be solved for the macro-displacement field $\bar{\mathbf{u}} = \{\bar{u}, \bar{v}\}^T$. The near-tip elasticity solutions for homogeneous orthotropic cracked bodies have been obtained by Sih *et al.* (1965) and Kaczynski and Matysiak (1989). The solution by Sih *et al.* is presented in the Appendix with minor modifications. As discussed during the formulation of the non-standard elasticity problem for heterogeneous systems, the near-tip homogeneous orthotropic solution can be used to represent the macro-displacements $\bar{u}$, $\bar{v}$ for the heterogeneous region shown in Fig. 3. In doing so, the compliance matrix $[b_{ij}]$ $(i,j = 1,2,6)$ used by Sih *et al.* is taken as the inverse of the effective elastic stiffness matrix $[C_{ij}]$ developed in eqn (15) for the homogenized domain. Thus, the micro-displacement field can be obtained at any point of the solution domain with the aid of eqns (1)–(2), (4) and (13). Thus, the micro-displacements in the heterogeneous medium take the following form:

$$u^{(m)} = \bar{u} - \frac{1}{v_m}(x - x_m)(a_1\bar{u}_{,x} + a_2\bar{v}_{,y})$$

$$v^{(m)} = \bar{v} - \frac{c_3}{v_m}(x - x_m)(\bar{u}_{,y} + \bar{v}_{,x}) \tag{16}$$

in the matrix phase and

$$u^{(f)} = \bar{u} + \frac{1}{v_f}(x - x_f)(a_1\bar{u}_{,x} + a_2\bar{v}_{,y})$$

$$v^{(f)} = \bar{v} + \frac{c_3}{v_f}(x - x_f)(\bar{u}_{,y} + \bar{v}_{,x}) \tag{17}$$

in the fiber phase where a_1, a_2 and a_3 are material constants which depend on the elastic mismatch in the unit-cell. These constants for the bimaterial system under consideration are given by:

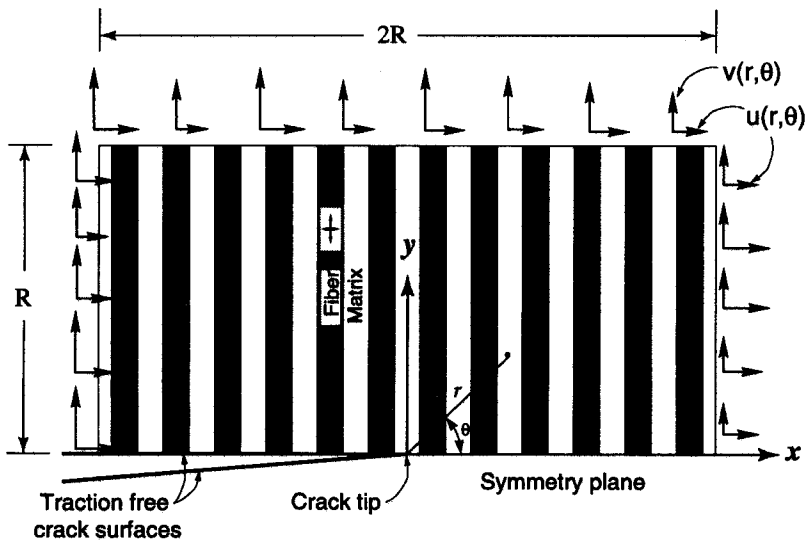

Fig. 3. The plane strain boundary value problem used for the near-tip finite element studies.

$$a_1 = \left(\frac{c_{11}^m - c_{11}^f}{\frac{c_{11}^m}{v_m} + \frac{c_{11}^f}{v_f}}\right), \quad a_2 = \left(\frac{c_{12}^m - c_{12}^f}{\frac{c_{11}^m}{v_m} + \frac{c_{11}^f}{v_f}}\right), \quad a_3 = \left(\frac{c_{66}^m - c_{66}^f}{\frac{c_{66}^m}{v_m} + \frac{c_{66}^f}{v_f}}\right).$$

The elastic micro-strains at every point in the heterogeneous solution domain can be now obtained with the aid of eqn (5). However, the terms containing the products of the shape function with the derivatives of micromorphic parameters $g_i(x, y)$ in eqn (5) are comparatively small and can be neglected. It is worth mentioning here that whereas the presence of these terms improves the accuracy of σ_{yy}, it introduces small but non admissible traction discontinuities at the interfaces. Using eqn (5) and after neglecting terms containing derivatives of $g_i(x, y)$, the expressions for the non-zero strains in the matrix phase are obtained as:

$$\begin{aligned}
\varepsilon_{xx}^{(m)} &= \bar{u}_{,x} - \frac{1}{v_m}(a_1 \bar{u}_{,x} + a_2 \bar{v}_{,y}) \\
\varepsilon_{yy}^{(m)} &= \bar{v}_{,y} \\
\gamma_{xy}^{(m)} &= \left(1 - \frac{a_3}{v_m}\right)(\bar{u}_{,y} + \bar{v}_{,x})
\end{aligned} \tag{18}$$

whereas in the fiber phase they are given by:

$$\begin{aligned}
\varepsilon_{xx}^{(f)} &= \bar{u}_{,x} + \frac{1}{v_f}(a_1 \bar{u}_{,x} + a_2 \bar{v}_{,y}) \\
\varepsilon_{yy}^{(f)} &= \bar{v}_{,y} \\
\gamma_{xy}^{(f)} &= \left(1 + \frac{a_3}{v_f}\right)(\bar{u}_{,y} + \bar{v}_{,x}).
\end{aligned} \tag{19}$$

The micro-stresses in a particular layer of the solution domain can be obtained through the following local stress–strain relations:

$$\sigma_i^{(n)} = c_{ij}^{(n)} \varepsilon_j^{(n)} \quad i, j = 1, 2, 6 \tag{20}$$

where the superscript n in parentheses designates the layer within which the equations are applied. As before, in the above equations summation over the designated range of 1, 2 and 6 is implied by the repeated index j. After combining eqns (18), (19) and (20), the micro-mechanical stresses take the following form:

$$\begin{aligned}
\sigma_{xx}^{(n)} &= C_{11} \bar{\varepsilon}_{xx} + C_{12} \bar{\varepsilon}_{yy} \\
\sigma_{yy}^{(n)} &= \frac{c_{12}^{(n)}}{c_{11}^{(n)}} C_{11} \bar{\varepsilon}_{xx} + \left[c_{22}^{(n)} + \frac{c_{12}^{(n)}}{c_{11}^{(n)}}(C_{12} + c_{12}^{(n)})\right] \bar{\varepsilon}_{yy} \\
\sigma_{xy}^{(n)} &= C_{66} \bar{\gamma}_{xy}.
\end{aligned} \tag{21}$$

Clearly, we notice that the stress components $\sigma_{xx}^{(n)}$ and $\sigma_{xy}^{(n)}$ depend only on the homogenized stiffnesses and they are, in fact, identical to the homogeneous orthotropic stresses $\bar{\sigma}_{xx}$ and $\bar{\sigma}_{xy}$. This result automatically enforces traction continuity along all matrix/fiber interfaces. For the crack-tip fields in the periodically layered systems, the macro displacements $\bar{u}$, $\bar{v}$ and their derivatives in eqns (16)–(21) are taken to be those obtained by Sih *et al.* (1965).

4. NEAR-TIP FINITE ELEMENT MODEL

The near-tip boundary value problem is shown in Fig. 3, which represents the *cut-out* region (see Fig. 1) surrounding the physical crack-tip of a macroscopic mode-I crack embedded at 90-degree to the interfaces of a laminate compact tension, centered crack plate or even a double cantilever beam specimen. The boundary of the *cut-out* domain shown in Fig. 3, is assumed to be within the region dominated by the homogeneous orthotropic stress intensity factor, K_I^o. This clearly requires that the dimension R of the *cut-out* region is both sufficiently larger than the characteristic microstructural length and also sufficiently smaller than a characteristic macroscopic specimen dimension such as the crack length or specimen height or uncracked ligament size. As shown in Fig. 3, the physical dimensions of the near-tip region were taken to be $2R \times 2R$. The near-tip solution domain comprises of alternating layers of the *matrix* and the *fiber* consistent with the lamination morphology used in the development of the analytical approximate model. While the crack surfaces were considered traction free, symmetry boundary conditions consistent with mode-I loading, namely zero displacement in the y-direction and zero force in the x-direction, were imposed at all nodes ahead of the crack-tip. The asymptotic mode-I homogeneous orthotropic displacements were imposed on the remaining part of the boundary. This displacement field, which is characterized by the remote orthotropic stress intensity factor K_I^o, has the following form:

$$\begin{Bmatrix} u \\ v \end{Bmatrix} = K_I^0 \sqrt{\frac{r}{2\pi}} \operatorname{Re} \begin{Bmatrix} U(\theta, b_{ij}) \\ V(\theta, b_{ij}) \end{Bmatrix}, \tag{22}$$

where r and θ are the polar coordinates as shown in Fig. 3, b_{ij} are compliancies of the homogeneous orthotropic medium, and U and V are the spatial complex eigen-functions obtained by solving the near-tip mode-I asymptotic problem for a homogeneous orthotropic medium. The explicit forms for U and V are given in the Appendix.

The layered *cut-out* region was discretized using sufficient number of eight-noded isoparametric elements as needed to capture high stress gradient fields. A typical finite element mesh used in this study is shown in Fig. 4. In order to investigate the effects of dual length ratio R/l [Ballarini *et al.* (1995)] and the crack-tip location with respect to the matrix/fiber interface, various meshes were constructed using an automated mesh generator for the layered systems. In all cases, a focused mesh was used in the immediate vicinity of the crack-tip which was surrounded by a rosette of singular quarter point elements to capture the expected square root singular stresses. The near-tip finite element solutions were obtained using the in-house finite element software DENDRO and the commercially available finite element package ABAQUS. A full integration scheme was used in the integration of the element stiffnesses.

5. RESULTS

In this section, the near-tip field quantities predicted by the analytical approximate model and those obtained numerically via the method of finite elements are presented. The model and finite element predictions are compared with each other and with the known near-tip analytical solution for isotropic and homogeneous orthotropic media. As discussed earlier in this work, overall plane strain conditions were considered. Thus, it was assumed that the out-of-plane thickness of the layered system was sufficiently large compared to a specimen characteristic length such that the conditions of plane strain prevailed in the interior away from the lateral traction free surfaces.

The results presented in this section were obtained for a bimaterial layered system comprised of alternating isotropic elastic layers. As mentioned earlier, the softer material is referred to as the *matrix* phase and the stiffer material is referred to as the *fiber* phase. Results were obtained for various moduli ratios $\lambda = E_f/E_m$ and fiber volume fractions v_f, where subscripts f and m represent properties for the fiber and the matrix phases, respectively. In all cases, the Poisson's ratio for each layer was taken to be $\nu_f = \nu_m = 0.3$. Without

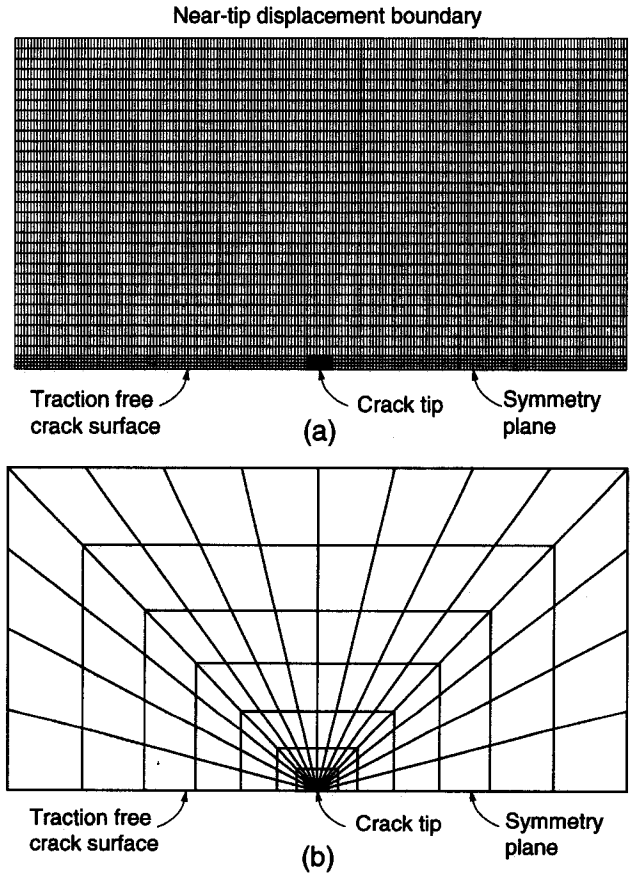

Fig. 4. (a) A finite element mesh used in solving the near-tip boundary value problem shown in Fig. 3. (b) Details of the focused near-tip mesh.

loss of generality, most of the results presented in this paper correspond to $\lambda = 10$ and fiber volume fraction $v_f = 0.5$. In order to investigate the effects of the actual number of layers in the laminate on the near-tip mechanics, systems with dual length ratios $R/l = 5$, 10, 25 and 50 were considered. The stresses are normalized with the reference stress $\sigma_o = K_I^o/\sqrt{2\pi R}$, while the displacements are normalized with the reference displacement $U_o = K_I^o/E_o\sqrt{R/2\pi}$, and the spatial distance is normalized with a reference length R. As before, K_I^o represents the homogeneous orthotropic mode-I stress intensity factor and E_o is the reference modulus which for this study is taken to be the matrix modulus E_m.

5.1. *Near-tip displacements*

The radial variation of the normalized displacements at an angular position $\theta = 45°$ are shown in Fig. 5(a). The displacement components as obtained by finite element analysis were found to oscillate around the corresponding homogeneous orthotropic displacements. The approximate analytical model predicted the displacement field quite accurately throughout the solution domain with some deviations observed within the first unit-cell from the crack-tip. The angular variation of the normalized displacements at a radial distance $r/R = 0.8$ is shown in Fig. 5(b). It is observed that the proposed model is capable of capturing the displacement field fairly well over the entire angular region.

5.2. *Normal stress ahead of the crack-tip*

Profiles for the normalized σ_{yy} acting on the plane ahead of the crack-tip are shown in Fig. 6. The results are plotted on a log–log scale such that the slope of the stress profile indicates the strength of the dominant singularity. Results for systems of dual length ratios $R/l = 5$, 10, 25 and 50 are reported in Fig. 6(a)–(d). For comparison purposes, the analytical homogeneous orthotropic stress predictions are also presented. In the above figures, the heavy solid line represents the homogeneous orthotropic singular stress, the thin continuous

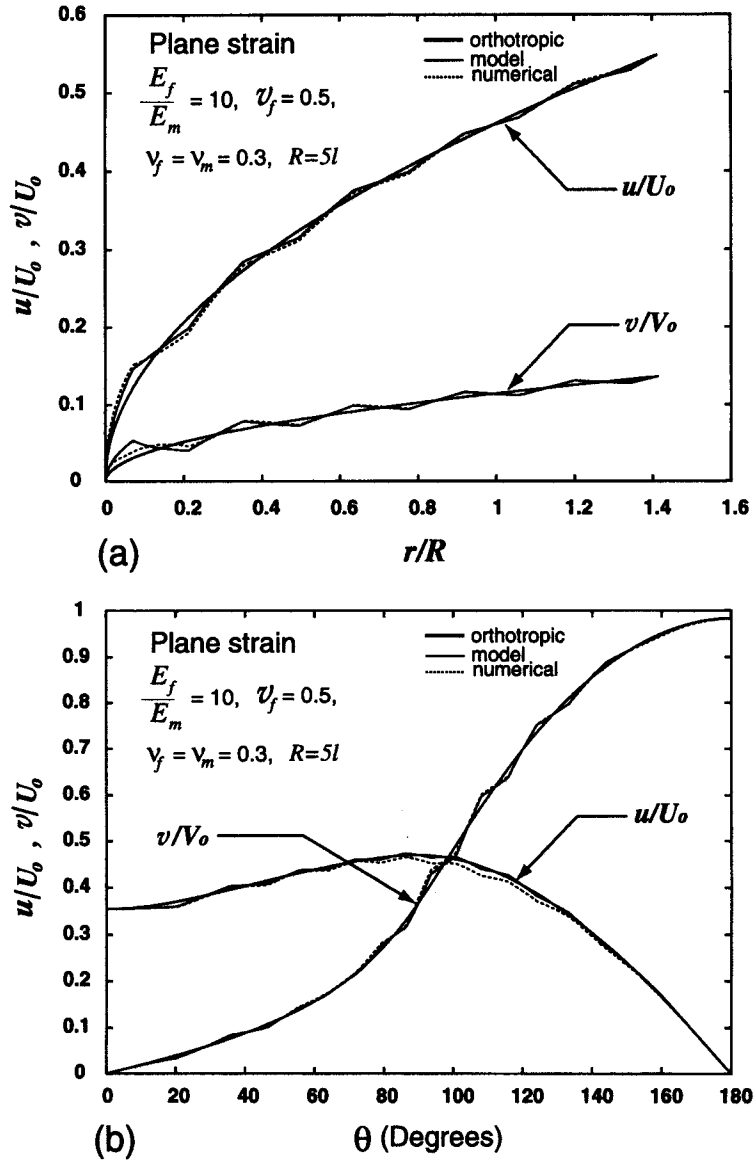

Fig. 5. (a) Radial variations of displacements at an angle $\theta = 45°$. (b) Angular variations of displacements at a distance $r = 0.8R$ from the crack-tip.

line represents the approximate model prediction while the dotted line represents the finite element results. The unit-cell average results were obtained by integrating the finite element microstresses across a fiber/matrix unit-cell and dividing by the length of the unit-cell consistent with Ballarini *et al.* (1995). As expected, for all systems considered, the stress profiles are discontinuous at the fiber/matrix interfaces due to the elastic modulus mismatch between the two material phases and the stress in the compliant matrix phase is consistently lower compared to that in the stiffer fiber phase. Again for all systems considered, the stress in the immediate vicinity of the crack-tip exhibits an $r^{-1/2}$ variation almost up to the first interface ahead of the crack-tip. In the subsequent fiber and matrix layers, the local micro stress distribution appears to deviate from the $r^{-1/2}$ dependency mainly due to the effects of strong material heterogeneity. However, the overall stress pattern in the matrix as well as in the fiber phases seems to be confined within an $r^{-1/2}$ singular envelope which is nicely captured by the analytical approximate model. This observation suggests that the microstress σ_{yy} in the fiber and the matrix phases is dominated by the orthotropic stress intensity factor and a discontinuous spatial eigen-function which accounts for the observed stress discontinuities. As shown in Fig. 5, the near-tip heterogeneous stresses predicted by the approximate analytical model match very closely with the finite element solution. It is

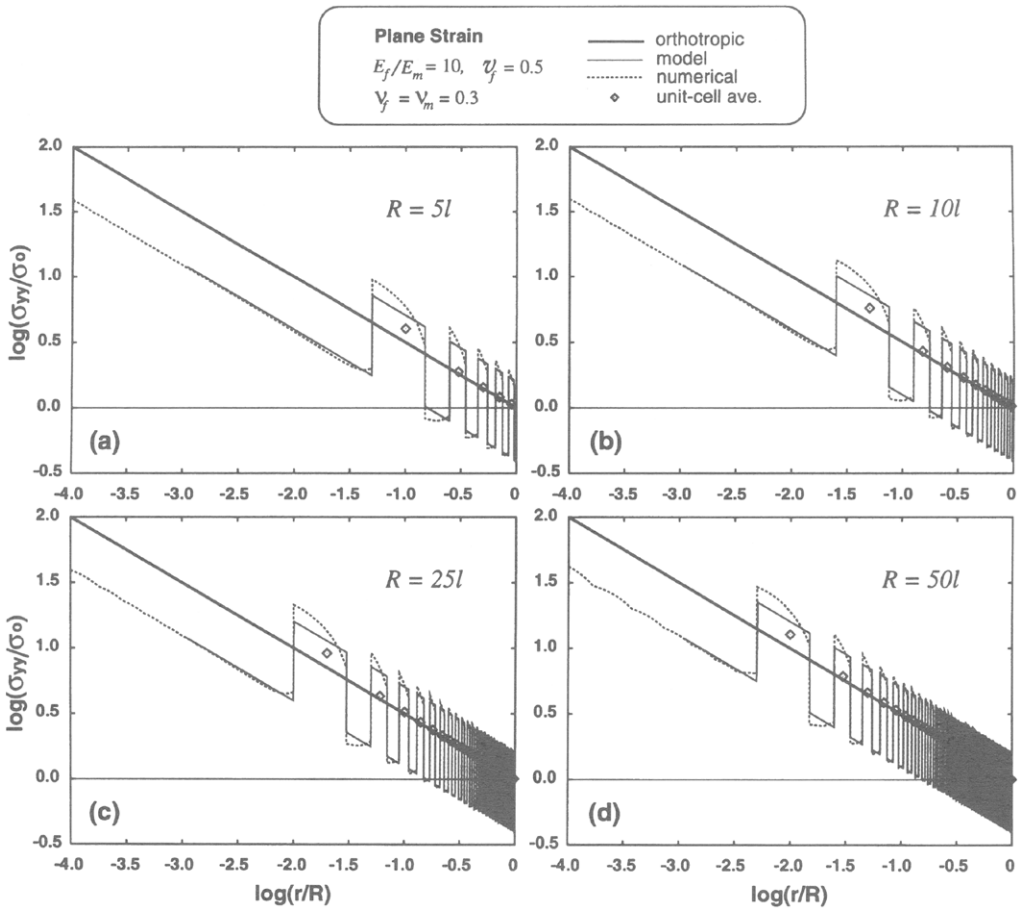

Fig. 6. Normal stress profiles ahead of the crack-tip.

to be noted here that the $r^{-1/2}$ stress singularity of the model results from the homogeneous orthotropic near-tip displacement field which inherently contains this feature.

5.3. *Angular micro-stress profiles*

The angular variations of the normalized micro-stress components σ_{xx}/σ_o, σ_{yy}/σ_o and σ_{xy}/σ_o at a normalized radial distance $r/R = 0.001$ as a function of angular position θ are presented in figure columns 7(a) through 7(c). Since this region falls entirely within the matrix phase surrounding the physical crack-tip, the isotropic singular solution is also plotted. The tip stress intensity factor $K_I^{tip} = 0.4K_I^o$ was obtained by matching the analytical isotropic stress $\sigma_{yy}(x, 0)$ at the crack-tip with that obtained by the finite element calculations. It was found that the stress field in the immediate vicinity of the crack-tip exhibits almost isotropic behavior. Through separate studies [Jha *et al.* (1995)] it has been shown that the tip stress intensity factor K_I^{tip} is strongly dependent on the crack-tip location with respect to the adjacent matrix/fiber interfaces. As shown in Fig. 7(a)–(c), in high dual length ratio systems, i.e., $R/l = 25$ [see Fig. 7(c)], the values of σ_{xx} appear to deviate slightly from their equivalent isotropic results. This deviation is to be expected since the region dominated by the isotropic field diminishes with increasing dual length ratio R/l. The results reported in Fig. 7 are obtained at a fixed distance $r/R = 0.001$ from the crack-tip and as such, the slight deviation shown by the σ_{xx}-component in 7(c) may reflect the effects of the diminishing isotropic zone with R/l.

The angular variation of the normalized micro-stress components σ_{xx}/σ_o, σ_{yy}/σ_o and σ_{xy}/σ_o at a normalized radial distance $r/R = 0.8$ are shown in figure columns 8(a) through 8(c). While the stress field dominating the matrix material in the immediate vicinity of the crack-tip was found to be consistent with the isotropic fields and exhibited sensitivity to the location of the physical crack-tip, the stresses away from the crack-tip at radial distances

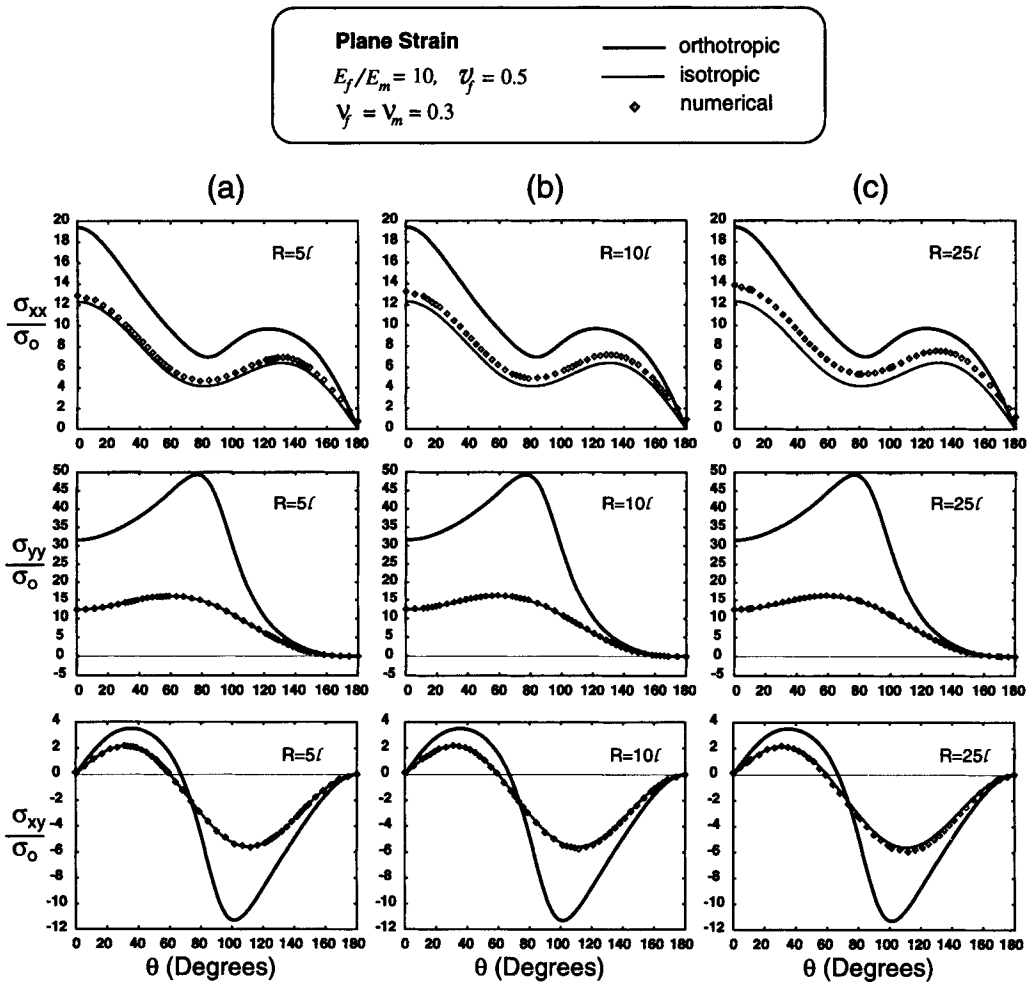

Fig. 7. Angular stress profiles in the vicinity of the crack-tip at a radial distance $r = 0.001R$ from the tip.

beyond one unit-cell thickness, were found to be unaffected by the actual tip location relative to the adjacent matrix/fiber interfaces. Consistent with the heterogeneous micro structure, σ_{yy} is found to be discontinuous at the matrix/fiber interfaces. While the continuous stress components σ_{xx} and σ_{xy} are shown to be in good agreement with their orthotropic counterparts, the discontinuous stress σ_{yy} is found to oscillate around the homogeneous orthotropic solution. This oscillation of σ_{yy} arising from the material heterogeneities is very nicely captured by different eigen-functions associated with the matrix and the fiber phases. For all systems considered, the predictions of the approximate analytical model were found to be in a remarkable agreement with the finite element solutions. This enforces confidence in the approximate model which can be used to extract additional information regarding the structure of the micro-stress fields and their implications on mode-I fracture in layered systems.

5.4. *Radial profiles of σ_{yy} stress*

The stress profiles along several radii emanating from the physical crack-tip are shown in Fig. 9. As before, the results presented here are those for a layered system with moduli ratio $\lambda = 10$, $\nu_f = \nu_m = 0.3$, fiber volume fraction $v_f = 0.5$ and dual length ratio $R/l = 10$. The results shown in Fig. 9 correspond to radii at angular positions $\theta = 0$, 30, 45, 60, 120 and 135 degrees, respectively. The discontinuities in σ_{yy} are consistent with the matrix/fiber interface locations. As evident from the above results and the results shown in Fig. 7, the oscillating characteristic of σ_{yy} is found due to the presence of a discontinuous spatial eigenfunction that describes σ_{yy} in bimaterial layered systems. As shown, the approximate model is in remarkable agreement with the finite element results.

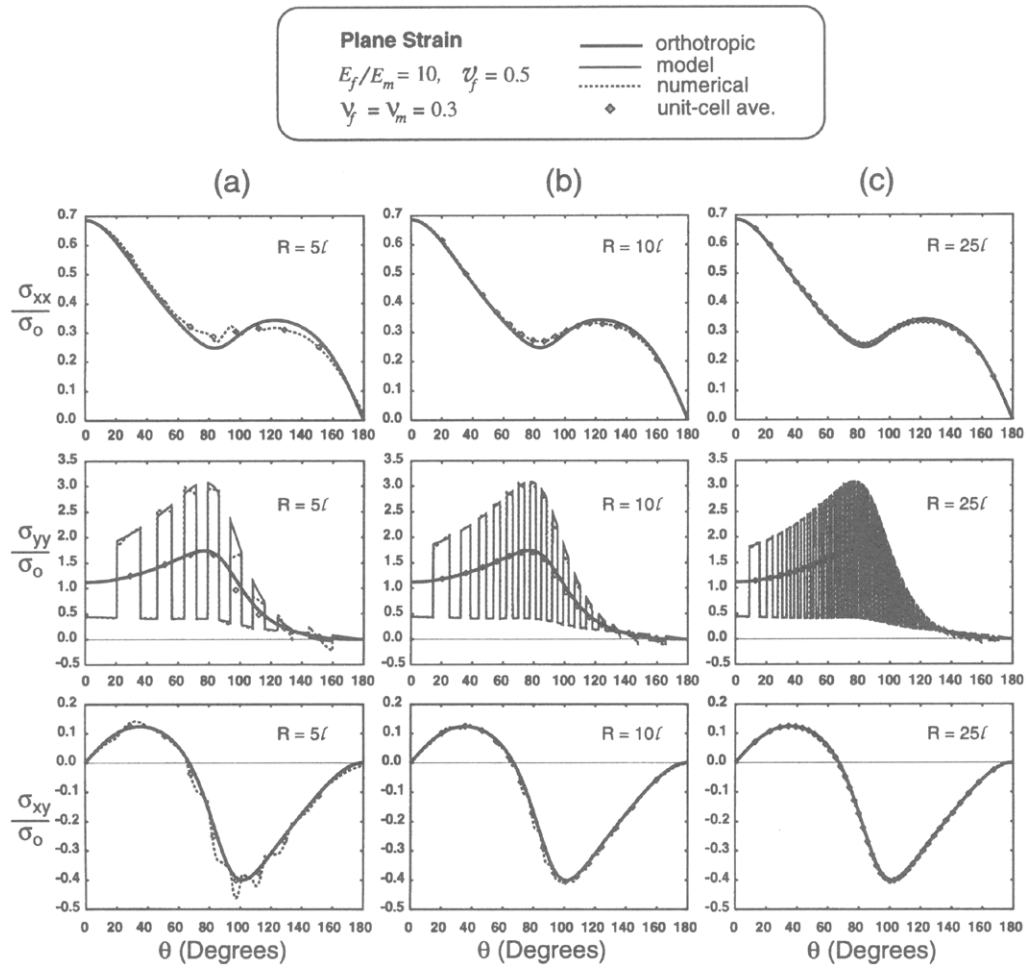

Fig. 8. Angular stress profiles at a distance $r = 0.8R$ from the crack-tip. The model and homogeneous orthotropic predictions for σ_{xx} and σ_{xy} are identical and thus overlap. Similar effects may be observed in some cases when comparing the model and finite element results.

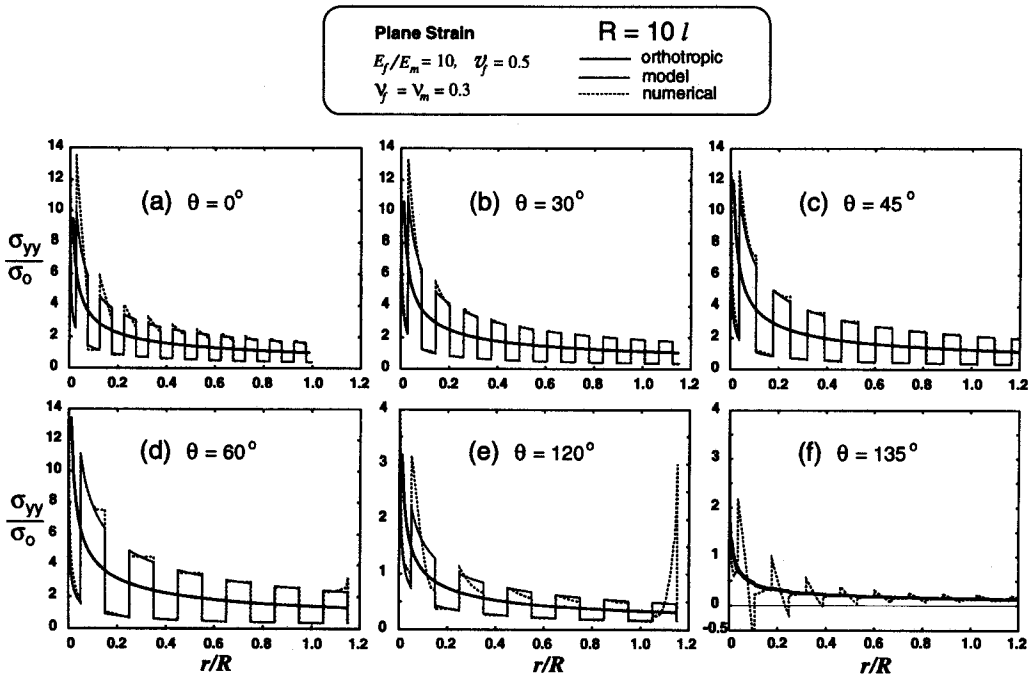

Fig. 9. Radial profiles of stress component σ_{yy} for different angular positions.

6. DISCUSSIONS

The results reported in Figs 6–9 provide meaningful insights on the mode-I near-tip mechanics in layered systems. The results of this investigation suggest that the near-tip region in layered systems is dominated by three distinct stress fields. More specifically, the stress fields in the matrix region surrounding the crack-tip appear to be those obtained for isotropic systems. On the other hand, the stress fields in the outer near-tip annulus domain appear to be the part of an overall $r^{-1/2}$ singular field dominated by the orthotropic stress intensity factor. The inner and the outer K-dominated fields are linked through a narrow transition zone, the extent of which appears to be limited to approximately one fiber/matrix unit-cell length. The elastic fields in these three regions and their implications on fracture are discussed in the following subsections.

6.1. *Elastic fields in the innermost region I*

As discussed by Charalambides (1991) and Ballarini *et al.* (1995), the extent of the innermost zone is limited by a characteristic micro-length such as the spacing b between the crack-tip and the first matrix/fiber interface as shown in Fig. 10. This study suggests that material points within region-I bounded by a radius $r_1 \approx (0.01-0.1)l_m$ are dominated by the isotropic asymptotic K-field the structure of which is not affected by the heterogeneous micro-structure. While the spatial variation of the elastic fields in region-I is shown to be that of the isotropic fields, the dominant stress intensity factor K_I^{tip} is found to depend on the heterogeneous micro-structure of the layered system. This dependency was first reported by Ballarini *et al.* (1995) and it has been verified through the present studies. While Ballarini *et al.* (1995) reported numerically obtained discrete values of the relationship between K_I^{tip} and the remotely applied K_I^o, the analytical approximate model developed in the present study can be used to establish this relationship. As observed in Fig. 6, σ_{yy} appears to be dominated by the same stress intensity factor in the matrix region-I as well as in all other matrix layers. This observation has very strong implications as the tip stress intensity factor K_I^{tip}, at least for the geometry under consideration, can be defined as:

$$K_I^{tip} = \lim_{r\to 0} \sqrt{2\pi r}\sigma_{yy}^m(r,0). \tag{23}$$

In isotropic bimaterial layered systems, the expression for σ_{yy}^m given in eqn (21) can be rewritten in the reduced form:

$$\sigma_{yy}^m = \frac{\nu_m}{1-\nu_m}\sigma_{xx}^m + \frac{E_m}{1-\nu_m^2}\bar{\varepsilon}_{yy}. \tag{24}$$

Here, ν_m and E_m represent the Poisson's ratio and the elastic modulus of the matrix material

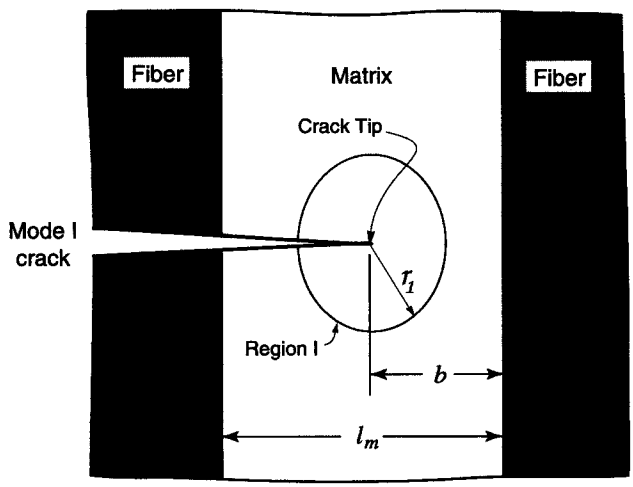

Fig. 10. A schematic representation of the small singular region I surrounding the crack-tip in bimaterial layered systems.

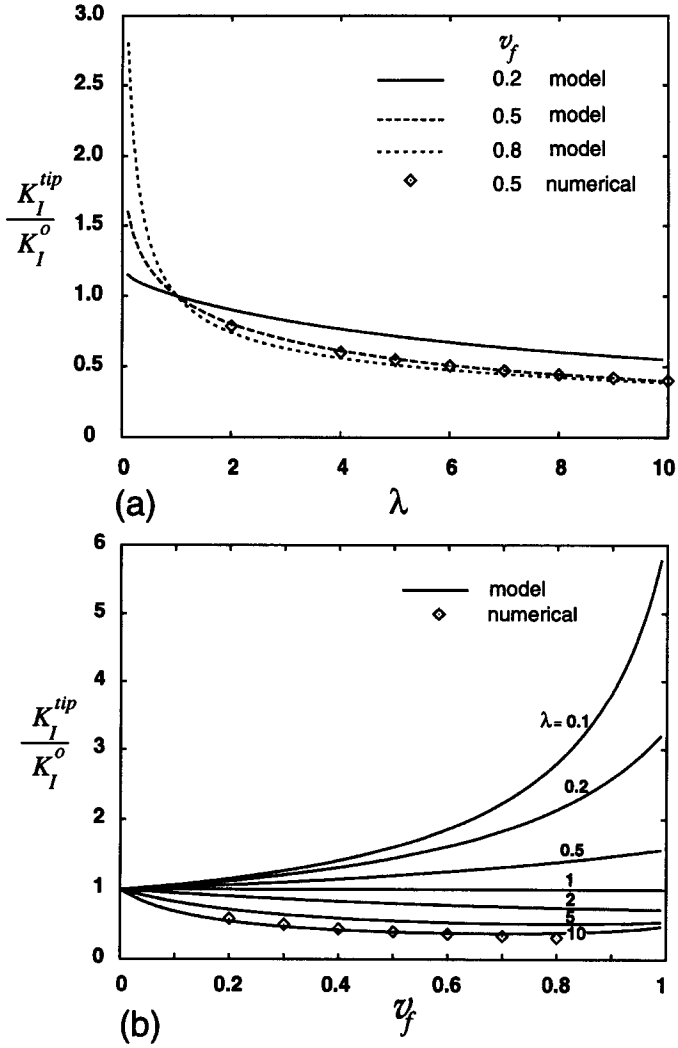

Fig. 11. The tip stress intensity factor (a) as a function of moduli ratio λ (b) as a function of the fiber volume fraction v_f.

respectively. The model prediction for the continuous stress component σ_{xx} is identical to that predicted by the homogeneous orthotropic solution, so it can be replaced by the first equation of (A.3) in the Appendix. Similarly, the average strain $\bar{\varepsilon}_{yy}$ can also be expressed in terms of the homogeneous orthotropic stress intensity factor. With the above substitutions and further simplification, the tip stress intensity factor can be obtained with the aid of eqn (23) as:

$$K_I^{tip} = \Gamma_I K_I^o \tag{25}$$

where Γ_I is a non-dimensional function which depends implicitly on material constants λ, v_m, v_f and the fiber volume fraction v_f and is obtained as the real part of a complex function of the above properties as follows:

$$\Gamma_I = \mathrm{Re}\left[\frac{\mu_1\mu_2}{\mu_1-\mu_2}\left(\frac{v_m(\mu_2-\mu_1)}{1-v_m}+\frac{E_m(q_2-q_1)}{1-v_m^2}\right)\right]. \tag{26}$$

In eqn (26) μ_1, μ_2 are the roots of the characteristic eqn (A.5) given in the Appendix and q_1, q_2 are those defined by eqn (A.6).

The effects of the moduli ratio λ and the fiber volume fraction v_f on the tip stress intensity factor K_I^{tip} are shown in Fig. 11. In Fig. 11(a), the normalized tip stress intensity

factor is plotted against the moduli ratio λ for various fiber volume fractions v_f. The above results were obtained assuming that the crack-tip was located in the middle of the matrix phase. The discrete points in the above figure represent finite element predictions for a system wherein $v_f = 0.5$. It is observed from Fig. 11(a) that by increasing the fiber volume fraction, higher shielding effects are produced for $\lambda > 1$ while amplification takes place for $\lambda < 1$. It is interesting to note that the rate of increase of amplification with respect to the fiber volume fraction is higher compared to the rate at which shielding increases. For $\lambda > 1$, we find a remarkable agreement between the model prediction and the numerical results. The tip stress intensity factor against fiber volume fraction is shown in Fig. 11(b). The model predictions are reported for $\lambda = 0.1, 0.2 \ldots 10$ while the finite element results in Fig. 11(b) correspond to $\lambda = 10$. A good agreement is found between the model and the finite element results over the full range of fiber volume fraction.

6.2. *Elastic fields in the outermost region III*

As discussed above, the isotropic stress intensity factor K_I^{tip} given by eqn (25), dominates the elastic fields in region-*I* shown in Fig. 10. While the above finding applies to a relatively very small region surrounding the crack-tip (see Fig. 10), the stresses at radial distances greater than a fiber/matrix unit cell length have been shown to be dominated by the applied orthotropic stress intensity factor K_I^o. The stress components σ_{xx} and σ_{xy} in region-*III* are continuous and are found to be in good agreement with their homogeneous orthotropic counterpart. The σ_{yy} is described by a discontinuous spatial eigen-function which accounts for the observed discontinuities. As demonstrated earlier in this study, the above behavior is captured by the analytical approximate model. With the aid of the approximate model, it can be shown that the continuous stress components in region-*III* are given by:

$$\sigma_{xx} = \frac{K_I^o}{\sqrt{2\pi r}} F_{xx}(\lambda, v_f, v_f, v_m, \theta) \tag{27}$$

$$\sigma_{xy} = \frac{K_I^o}{\sqrt{2\pi r}} F_{xy}(\lambda, v_f, v_f, v_m, \theta) \tag{28}$$

where $F_{xx}(\cdot)$ and $F_{xy}(\cdot)$ are eigen-functions identical to those reported in the Appendix for the homogeneous orthotropic problem. Similarly, the discontinuous stress σ_{yy} can be expressed as:

$$\sigma_{yy} = \frac{K_I^o}{\sqrt{2\pi r}} F_{yy}(\lambda, v_f, v_f, v_m, \theta) \tag{29}$$

where $F_{yy}(\cdot)$ is a piece-wise continuous spatial eigen-function which exhibits discontinuities at all matrix/fiber interfaces. For plane strain, the explicit form of the discontinuous eigen-function for layer type j is given by:

$$F_{yy}^j = \frac{1}{(1-v_j)} \mathrm{Re}\left[\frac{\mu_1\mu_2}{\mu_1-\mu_2}\left(\frac{v_j\mu_2 + E_j q_2/(1+v_j)}{\sqrt{\cos\theta+\mu_2\sin\theta}} - \frac{v_j\mu_1 + E_j q_1/(1+v_j)}{\sqrt{\cos\theta+\mu_1\sin\theta}}\right)\right]. \tag{30}$$

Obviously, F_{yy}^j changes with the change in material phase and eigen-functions for the matrix and fiber phases are obtained by allowing the index j to become either m for the matrix or f for the fiber phases in the above equation. Thus, the stress and deformation fields in the outermost region-*III*, can be fully described via the orthotropic stress intensity factor K_I^o and the spatially discontinuous eigen-function $F_{yy}(\cdot)$.

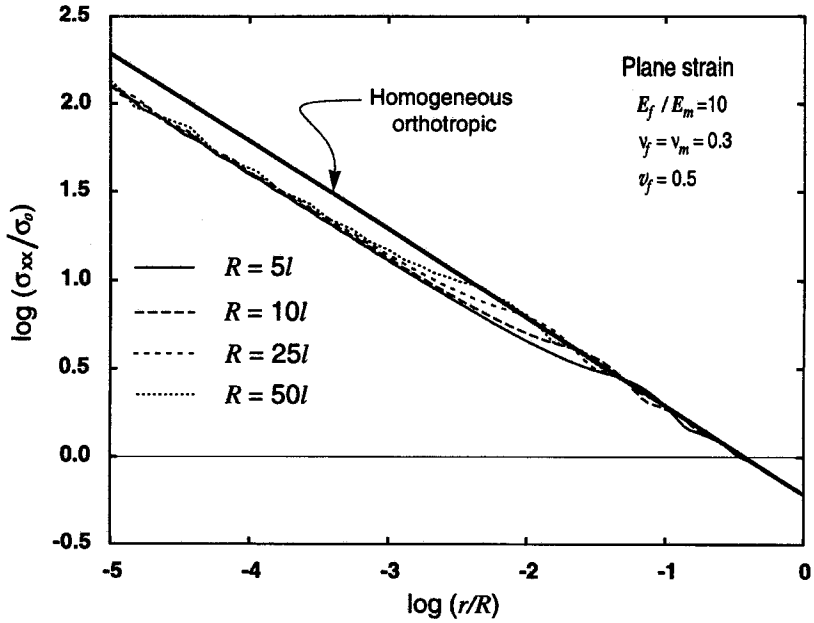

Fig. 12. Stress component σ_{xx} ahead of the crack-tip as predicted by the finite element model.

6.3. *Elastic fields in the transition region II*

While the approximate analytical model does not allow for an intermediate transition stress fields, the refined finite element results support the existence of this region. As an evidence to this fact, the normalized σ_{xx} stress component ahead of the crack-tip has been plotted against the normalized distance on a log–log scale in Fig. 12. It is noticed that the isotropic field dominating the matrix region in the immediate vicinity of the crack-tip (see Fig. 10) changes very rapidly to the field dominating the outermost annular region. As shown by this study and the study by Ballarini *et al.* (1995) the transition from region-*I* to region-*III* takes place within the first fiber/matrix unit cell and appears to be slightly dependent on the dual length ratio. As discussed earlier in this work, it has been shown through complementary studies [Jha *et al.* (1995)] that the stress intensity factor dominating the near-tip fields in matrix region-*I* is sensitive to the crack-tip location relative to its adjacent matrix/fiber interfaces. The same complementary studies suggest that the remote stress fields in region-*III* are not affected by the actual crack-tip location within the matrix phase. As a result of the above observations, it is expected that the profiles of the elastic transition fields will depend on the actual crack-tip location within the matrix phase whereas the extent of the transition zone will be minimally affected by the actual crack-tip location.

6.4. *Implications on fracture*

As shown by this and other studies [Ballarini *et al.* (1995) and Fish *et al.* (1993)], a rather complex stress pattern exists in the crack-tip region of layered systems containing a crack oriented at 90-degree to the main layer direction. This stress pattern has direct implications on the process of mode-I fracture in layered brittle systems. As discussed earlier in this work, the elastic stresses in the matrix region-*I* in the immediate vicinity of the crack-tip (see Fig. 10) are dominated by the tip stress intensity factor K_I^{tip} given by eqns (25) and (26). Thus, the elastic energy release made available for brittle fracture of the matrix material in the crack-tip region is obtained via Irwin's relation as follows:

$$\mathcal{G}_I^{tip} = \frac{1-\nu_m^2}{E_m}(K_I^{tip})^2. \tag{31}$$

By replacing K_I^{tip} in the above equation with its equivalent given by eqn (25), $\mathcal{G}_I^{tip}$ takes the following form:

$$\mathcal{G}_I^{tip} = \frac{1-\nu_m^2}{E_m}\Gamma_I^2 (K_I^o)^2. \tag{32}$$

While the above equation predicts the near-tip energy release rate associated with the fields dominating the matrix material in region-*I* (see Fig. 10), for the same loading and specimen geometry (i.e., same K_I^o) different amounts of energy release rate are made available for composite fracture. Here, composite fracture implies that crack growth initiation as predicted through a Griffith failure criterion extends at least a matrix/fiber unit-cell. Such an event can be predicted by comparing the energy release rate estimated for the homogenized orthotropic medium $\mathcal{G}_I^o$, to an effective composite toughness $\mathcal{G}_{IC}^o$. As discussed by Sih *et al.* (1965), for given K_I^o, the associated energy release rate $\mathcal{G}_I^o$ is given by

$$\mathcal{G}_I^o = (K_I^o)^2 \sqrt{\frac{b_{11}b_{22}}{2}}\left[\sqrt{\frac{b_{22}}{b_{11}}} + \frac{2b_{12}+b_{66}}{2b_{11}}\right]^{1/2} \tag{33}$$

where $b_{ij} = [C_{ij}]^{-1}$ $(i,j = 1,2,6)$ represents the effective orthotropic elastic compliancies of the homogenized medium. The above equation can be rewritten as follows:

$$\mathcal{G}_I^o = \frac{1-\nu_m^2}{E_m}\Lambda_m(\lambda, v_f, \nu_m, \nu_f)(K_I^o)^2 \tag{34}$$

where Λ_m is a nondimensional function and E_m and ν_m are the Young's modulus and Poisson's ratio of the matrix material respectively. Under ideally brittle fracture conditions, fracture of the layered system may occur as a result of two possible failure events. In one possible failure event, crack growth initiation may first occur within the matrix region surrounding the crack-tip (see region-*I* in Fig. 10) while the fiber layers remain intact. In accordance with this failure scenario, crack extension entirely within the matrix may then follow the initiation of crack growth potentially leading to multiple matrix cracking with the bridging fibers still resisting catastrophic composite failure. Under increased applied loads, other events such as fiber layer debonding, fiber failure and fiber pull-out may precede the ultimate composite failure. While the above fracture processes may occur as a result of the initiation of matrix cracking prior to fiber failure, a second scenario exists wherein fiber failure may occur prior to matrix cracking initiation. Under this failure event, although the energy release rate made available to the matrix region-*I* at the crack-tip may not exceed the toughness of the matrix material for crack growth initiation, individual fibers ahead of the crack-tip may start failing. Such initial fiber failures may induce secondary failure events emanating at either the tips of the newly nucleated fiber cracks or at the tip of the major crack in the matrix region or at both tips simultaneously. In any case, when fiber failure occurs first, failure in the lower toughness matrix material becomes inevitable leading to brittle fracture of the entire composite. The exact order in which the above two failure events may occur can be assessed by applying Griffith's fracture energy criterion at the tip of the main crack as required to assess matrix failure while maintaining a below critical energy release rate for the homogenized composite. Thus, matrix failure prior to composite failure is predicted if:

$$\mathcal{G}_I^{tip} \geqslant \mathcal{G}_{IC}^m \quad \text{while} \quad \mathcal{G}_I^o < \mathcal{G}_{IC}^o \tag{35}$$

where $\mathcal{G}_{IC}^m$ and $\mathcal{G}_{IC}^o$ are the apparent fracture toughnesses of the matrix phase and the homogenized layered composite respectively, and $\mathcal{G}_I^{tip}$ and $\mathcal{G}_I^o$ are the respective energy release rates made available for the creation of new surfaces in the matrix region-*I* only and the broader homogenized tip region respectively. By dividing the above equations by parts, the following inequality for matrix failure over composite catastrophic fracture is obtained:

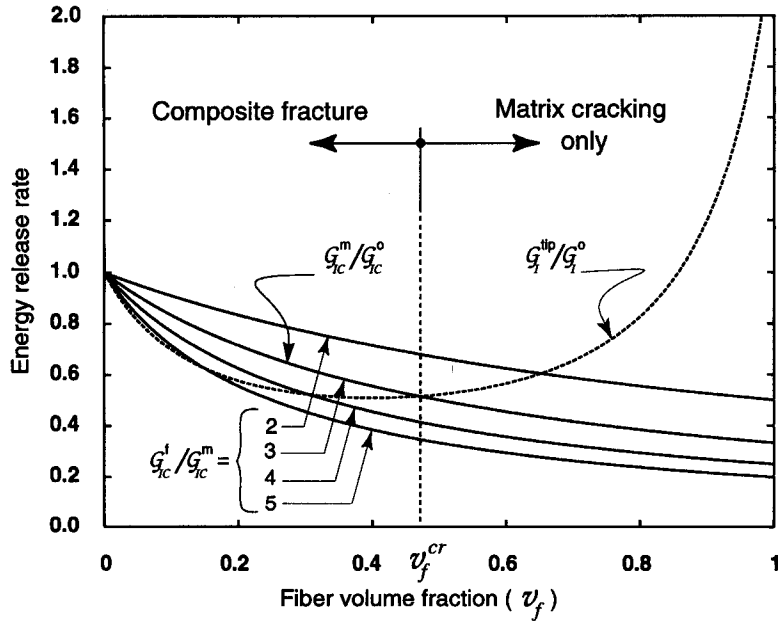

Fig. 13. Elastic energy release rate vs fiber volume fraction as predicted by the approximate analytical model for $\lambda = 10$.

$$\frac{\mathcal{G}_I^{tip}}{\mathcal{G}_I^{o}} \geqslant \frac{\mathcal{G}_{IC}^{m}}{\mathcal{G}_{IC}^{o}}. \tag{36}$$

In order to explore the above finding further, we shall consider an example system as follows. Let $\lambda = 10$ and $\mathcal{G}_{IC}^{f} = 3\mathcal{G}_{IC}^{m}$ where $\mathcal{G}_{IC}^{m}$ is the mode-I toughness of the matrix phase and $\mathcal{G}_{IC}^{f}$ is that of the fiber. During composite fracture, the new fracture surfaces generated can be multiplied by the respective matrix and fiber fracture energies to obtain the apparent composite toughness $\mathcal{G}_{IC}^{o}$ such that:

$$\mathcal{G}_{IC}^{o} = v_f\mathcal{G}_{IC}^{f} + (1-v_f)\mathcal{G}_{IC}^{m} \tag{37}$$

where v_f is the fiber volume fraction. By combining eqns (36) and (37) we obtain:

$$\frac{\mathcal{G}_I^{tip}}{\mathcal{G}_I^{o}} \geqslant \frac{1}{\dfrac{\mathcal{G}_{IC}^{f}}{\mathcal{G}_{IC}^{m}} v_f + (1-v_f)}. \tag{38}$$

For the system considered in this example, and after evaluating $\mathcal{G}_I^{tip}$ and $\mathcal{G}_I^{o}$ through eqns (32) and (34) respectively, the left and right hand side of eqn (38) can be independently plotted a shown in Fig. 13. For the example system under consideration the two curves intersect at a critical fiber volume fraction $v_f^{cr} = 0.47$. Clearly, in this example, for systems with fiber volume fraction v_f less than the critical value $v_f^{cr} = 0.47$ defined by the intersection of the two curves, the energy made available for composite failure exceeds the apparent composite toughness while the energy made available for matrix cracking remains below the critical value for matrix crack growth initiation. Therefore, when $v_f < v_f^{cr}$ and as indicated in Fig. 13, composite failure is predicted to occur prior to matrix cracking. On the other hand, when $v_f > v_f^{cr}$ then matrix cracking consistent with the first fracture event discussed earlier in this section is predicted to take place prior to composite failure. This may also suggest that as $\mathcal{G}_{IC}^{f}/\mathcal{G}_{IC}^{m}$ increases, critical fiber volume fraction v_j^{cr} decreases.

Clearly, the above discussion highlights the significance of being able to predict with sufficient accuracy the discontinuous microstress fields dominating the near-tip region of cracked layered systems. It is also understood that the actual events dominating fracture in

such complex systems will be significantly dependent on potential non-linear material responses such as microcracking damage in ceramics and ductile yielding in metal layers. Although, realistic fracture models are needed to account for such non-linear events, such studies are beyond the scope of this work which addressed the linear response and fracture behavior of cracked layered system under mode-I loading conditions.

7. CONCLUDING REMARKS

The micromorphic elastic fields in the near-tip region of a mode-I crack embedded at 90-degree to the layers in the periodically layered systems have been investigated using an approximate analytical model and the method of finite elements. The micro mechanical fields at radial distances greater than a fiber/matrix unit-cell were found to be dominated by the orthotropic stress intensity factor and a set of eigen-functions which account for the admissible stress discontinuities. An expression for the stress intensity factor, K_I^{tip}, which dominates the isotropic field in the matrix region-I surrounding the crack-tip has also been obtained. More specifically, K_I^{tip} was found to be related to the orthotropic stress intensity factor, K_I^o, via a material dependent function. In general, it has been shown that the singular micro mechanical elastic fields in such layered systems can be constructed from the homogeneous orthotropic field by introducing an *a priori* known shape function and certain unknown micromorphic parameters which take into account the effects of the micro-periodic material structure. The effective elastic constants for the homogenized medium are easily obtained by the assumed *a priori* known shape function and they are independent of both the unit-cell geometry and the amplitude of the shape function. The micro mechanical elastic fields predicted by the approximate analytical model match very closely with the finite element solution except in the region very near to the singular point, i.e., the crack-tip.

While the unit cell average stresses match very closely with the analytical homogeneous orthotropic solution, the actual singular stress fields in the laminated systems cannot be captured with homogenization. The approximate analytical model presented in this paper can be effectively utilized to predict the micro mechanical fields with sufficient accuracy in these periodically layered systems. The model can also be used to assess fracture initiation in brittle layered systems.

Acknowledgements—Support for this work was provided to M.J. and P.G.C. by the NSF through a Presidential Young Investigator award, grant CMS94-96209 and to R.B. through NSF grant CMS94-16752.

REFERENCES

Ballarini, R., Charalambides, P. G. and Islam, S. (1995) Near-tip dual length scale mechanics of mode-I cracking in laminated brittle matrix composites. *International Journal of Fracture* **70,** 275–304.

Ballarini, R. and Luo, H. A. (1991) Green's functions for dislocations in bonded strips and related crack problems. *International Journal of Fracture* **50,** 239–262.

Cao, H. C. and Evans, A. G. (1991) On crack extension in ductile/brittle laminates. *Acta Metallurgica* **39,** 2997–3005.

Charalambides, P. G. (1991) Steady state mechanics of delamination cracking in laminated ceramic-matrix composites. *Journal of the American Ceramic Society* **74,** 3066–3080.

Cook, T. S. and Erdogan, F. (1972) Stresses in bonded materials with a crack perpendicular to the interface. *International Journal of Engineering Science* **10,** 677.

Dalgleish, B. J., Trumble, K. P. and Evans, A. G. (1989) The strength and fracture of alumina bonded with aluminum alloys. *Acta Metallurgica* **37,** 1923–1931.

Delale, F. and Erdogan, F. (1988) On the mechanical modeling of the interfacial region in bonded half planes. *Journal of Applied Mechanics* **55,** 317–324.

Deve, H. E. and Maloney, M. J. (1991) On toughening of intermetallics with ductile fibers. *Acta Metallurgica* **39,** 2275–2284.

Erdogan, F. (1972) Fracture problems in composite materials. *Engineering Fracture Mechanics* **4,** 811–840.

Erdogan, F. and Biricikoglu, V. (1973) Two bonded half planes with a crack going through an interface. *International Journal of Engineering Science* **11,** 745–766.

Erdogan, F., Kaya, A. C. and Joseph, P. (1991) The crack problem in nonhomogeneous materials. *Journal of Applied Mechanics.* **58,** 410–418.

Fish, J., Fares, N. and Nath, A. (1993) Micromechanical elastic crack-tip stresses in a fibrous composite. *International Journal of Fracture* **60,** 135–146.

Gupta, V., Argon, A. S. and Sou, Z. (1992) Crack deflection at an interface between two orthotropic media. *Journal of Applied Mechanics* **59,** S79–S87.
He, M. Y. and Hutchinson, J. W. (1989) Crack deflection at an interface between dissimilar elastic materials. *International Journal Solids and Structures* **25,** 1053–1067.
Hutchinson, J. W. and Suo, Z. (1992) *Advances in Applied Mechanics*, Vol. 29.
Jha, M., Charalambides, P. G. and Ballarini, R. (1995) Crack-tip location effects on the near-tip mechanics in bimaterial layered systems. (In preparation.)
Kaczynski, A. and Matysiak, S. J. (1989) On crack problems in periodic two-layered elastic composites. *Engineering Fracture Mechanics* **32,** 745–756.
Lekhnitskii, S. G. (1963) *Theory of Elasticity of an Anisotropic Body*, Holden-Day, San Francisco.
Lu, M. C. and Erdogan, F. (1983) Stress intensity factors in two bonded elastic layers containing cracks perpendicular to and on the interface—I. analysis, II. solution and results. *Engineering Fracture Mechanics* **18,** 491–506; 507–528.
Martinez, D. and Gupta, V. (1993) Energy criterion for crack deflection at an interface between two orthotropic media—II. results and experimental verification. *Journal of Mechanics and Physics of Solids* **42** (MPS-81).
Matysiak, S. J. and Wozniak, Cz. (1987) Microlocal effects in a modeling of periodic multilayered elastic composites. *International Journal of Engineering Science* **25,** 549–559.
Suresh, S., Sugimura, Y. and Tschegg, E. K. (1992) The growth of a fatigue crack approaching a perpendicularly-oriented, bimaterial interface. *Scripta Metallurgica Materiala* **27,** 1189.
Sugimura, Y., Lim, P. G., Shih, C. F. and Suresh, S. (1995) Fracture normal to a bimaterial interface: effects of plasticity on crack-tip shielding and amplification. *Acta Metallurgica Materiala* **43,** 1157.
Swenson, D. O. and Rau, C. A., Jr. (1970) The stress distribution around a crack perpendicular to an interface between materials. *International Journal of Fracture Mechanics* **6,** 357–360.
Sih, G. C., Paris, P. C. and Irwin, H. (1965) On cracks in rectilinearly anisotropic bodies. *International Journal of Fracture Mechanics* **1,** 189–203.
Ting, C. T. C. and Hoang, P. H. (1984) Singularities at the tip of a crack normal to the interface of anisotropic layered composite. *International Journal of Solids and Structures* **20,** 439–454.
Tullock, D. L., Reimanis, I. E., Graham, A. L. and Petrovic, J. J. (1994) Deflection and penetration of cracks at an interface between two dissimilar materials. *Acta Metallurgica Materiala* **42,** 3245–3252.
Wozniak, Cz. (1987) A nonstandard method of modeling of thermoelastic periodic composites. *International Journal of Engineering Science* **25,** 483–498.
Zak, A. K. and Williams, M. L. (1963) Crack point singularities at a bi-material interface. *Journal of Applied Mechanics* **30,** 142–143.

APPENDIX

Near-tip fields in homogeneous orthotropic materials

For an anisotropic material, the generalized Hooke's law is given by

$$\varepsilon_i = s_{ij}\sigma_j \quad i,j = 1,2,6 \tag{A.1}$$

where $[s_{ij}] = [s_{ji}]$ is the compliance matrix for the material. When the material has a plane of elastic symmetry normal to z-axis, the Hooke's law for the deformation in the (x, y) plane [Lekhnitskii (1963)] reduces to

$$\varepsilon_i = b_{ij}\sigma_j \quad i,j = 1,2,6 \tag{A.2}$$

where

$$b_{ij} = \begin{cases} s_{ij} & \text{for plane stress} \\ s_{ij} - \dfrac{s_{i3}s_{j3}}{s_{33}} & \text{for plane strain} \end{cases}.$$

For the Mode-I loading considered in this paper, the stress and the displacement fields in the neighborhood of the crack-tip are given by [Sih *et al.* (1965)]

$$\bar{\sigma}_{xx} = \frac{K_I^o}{\sqrt{2\pi r}}\,\mathrm{Re}\left[\frac{\mu_1\mu_2}{\mu_1-\mu_2}\left(\frac{\mu_2}{\sqrt{\cos\theta+\mu_2\sin\theta}} - \frac{\mu_1}{\sqrt{\cos\theta+\mu_1\sin\theta}}\right)\right]$$

$$\bar{\sigma}_{yy} = \frac{K_I^o}{\sqrt{2\pi r}}\,\mathrm{Re}\left[\frac{1}{\mu_1-\mu_2}\left(\frac{\mu_1}{\sqrt{\cos\theta+\mu_2\sin\theta}} - \frac{\mu_2}{\sqrt{\cos\theta+\mu_1\sin\theta}}\right)\right]$$

$$\bar{\sigma}_{xy} = \frac{K_I^o}{\sqrt{2\pi r}}\,\mathrm{Re}\left[\frac{\mu_1\mu_2}{\mu_1-\mu_2}\left(\frac{1}{\sqrt{\cos\theta+\mu_1\sin\theta}} - \frac{1}{\sqrt{\cos\theta+\mu_2\sin\theta}}\right)\right] \tag{A.3}$$

$$\bar{u} = K_I^o\sqrt{\frac{2r}{\pi}}\,\mathrm{Re}\left[\frac{1}{\mu_1-\mu_2}(\mu_1 p_2\sqrt{\cos\theta+\mu_2\sin\theta} - \mu_2 p_1\sqrt{\cos\theta+\mu_1\sin\theta})\right]$$

$$\bar{v} = K_I^o\sqrt{\frac{2r}{\pi}}\,\mathrm{Re}\left[\frac{1}{\mu_1-\mu_2}(\mu_1 q_2\sqrt{\cos\theta+\mu_2\sin\theta} - \mu_2 q_1\sqrt{\cos\theta+\mu_1\sin\theta})\right] \tag{A.4}$$

where K_I^o is the Stress Intensity Factor and $\mu_j = \alpha_j + i\beta_j$ ($j = 1, 2$) are the roots (with $\beta_j > 0$) of the characteristic equation

$$b_{11}\mu^4 - 2b_{16}\mu^3 + (2b_{12} + b_{66})\mu^2 - 2b_{26}\mu + b_{22} = 0, \tag{A.5}$$

and

$$\begin{aligned} p_j &= b_{11}\mu_j^2 + b_{12} - b_{16}\mu_j \\ q_j &= b_{12}\mu_j + b_{22}/\mu_j - b_{26}. \end{aligned} \tag{A.6}$$

The partial derivatives of the displacements are given by:

$$\begin{aligned} \frac{\partial \bar{u}}{\partial x} &= \frac{K_I^o}{\sqrt{2\pi r}} \mathrm{Re}\left[\frac{1}{\mu_1 - \mu_2}\left(\frac{\mu_1 p_2}{\sqrt{\cos\theta + \mu_2 \sin\theta}} - \frac{\mu_2 p_1}{\sqrt{\cos\theta + \mu_1 \sin\theta}}\right)\right] \\ \frac{\partial \bar{u}}{\partial y} &= \frac{K_I^o}{\sqrt{2\pi r}} \mathrm{Re}\left[\frac{\mu_1\mu_2}{\mu_1 - \mu_2}\left(\frac{p_2}{\sqrt{\cos\theta + \mu_2 \sin\theta}} - \frac{p_1}{\sqrt{\cos\theta + \mu_1 \sin\theta}}\right)\right] \\ \frac{\partial \bar{v}}{\partial x} &= \frac{K_I^o}{\sqrt{2\pi r}} \mathrm{Re}\left[\frac{1}{\mu_1 - \mu_2}\left(\frac{\mu_1 q_2}{\sqrt{\cos\theta + \mu_2 \sin\theta}} - \frac{\mu_2 q_1}{\sqrt{\cos\theta + \mu_1 \sin\theta}}\right)\right] \\ \frac{\partial \bar{v}}{\partial y} &= \frac{K_I^o}{\sqrt{2\pi r}} \mathrm{Re}\left[\frac{\mu_1\mu_2}{\mu_1 - \mu_2}\left(\frac{q_2}{\sqrt{\cos\theta + \mu_2 \sin\theta}} - \frac{q_1}{\sqrt{\cos\theta + \mu_1 \sin\theta}}\right)\right]. \end{aligned} \tag{A.7}$$